Microscopy and Microanalysis, 2023, **29**, 326–333
https://doi.org/10.1093/micmic/ozac011
Advance access publication 15 December 2022
Original Article

Microscopy AND Microanalysis

Atomic-Scale Determination of Cation and Magnetic Order in the Triple Perovskite $Sr_3Fe_2ReO_9$

Ping-Luen Ho[1,2,a], Zhihao Huang[3,4,5,a], Lei Jin[6], Si-Young Choi[7], Rafal E. Dunin-Borkowski[6], Joachim Mayer[6,8], Shik Chi Edman Tsang[1] and Xiaoyan Zhong[3,4,5,*]

[1]*Wolfson Catalysis Centre, Inorganic Chemistry Laboratory, Department of Chemistry, University of Oxford, Oxford OX1 3QR, UK*
[2]*Department of Materials, University of Oxford, Oxford OX1 3PH, UK*
[3]*TRACE EM Unit and Department of Materials Science and Engineering, City University of Hong Kong, Kowloon 999077, Hong Kong SAR, People's Republic of China*
[4]*City University of Hong Kong Matter Science Research Institute (Futian, Shenzhen), Shenzhen 518048, People's Republic of China*
[5]*Nanomanufacturing Laboratory (NML), City University of Hong Kong Shenzhen Research Institute, Shenzhen 518057, People's Republic of China*
[6]*Ernst Ruska-Centre for Microscopy and Spectroscopy with Electrons (ER-C), Forschungszentrum Jülich GmbH, 52425 Jülich, Germany*
[7]*Department of Materials Science and Engineering, Pohang University of Science and Technology (POSTECH), Pohang 37673, South Korea*
[8]*Central Facility for Electron Microscopy, RWTH Aachen University, 52074 Aachen, Germany*

***Corresponding author:** Xiaoyan Zhong, E-mail: xzhong25@cityu.edu.hk

[a]These authors have contributed equally to this work.

Abstract

Pseudo-cubic (pc) perovskite oxides (ABO_3) that can have different magnetic cations with different types and degrees of order at B sites have attracted considerable interest as a result of their tunable magnetic properties. Nanoscale inhomogeneity in cation order on the B sites can lead to different magnetic ground states and electronic band structures in local sample regions. Here, we determine cation order on the atomic scale in a nanosized $Sr_3Fe_2ReO_9$ phase that has a 1:2 B-site-ordered triple perovskite structure using aberration-corrected analytical transmission electron microscopy (TEM), revealing that the Fe and Re cations form tripled-layered repeats with –[Fe–Fe–Re]$_n$– sequences along $[111]_{pc}$ and an ordering vector of 1/3[111]*. To the best of our knowledge, this 1:2 B-site-ordered triple perovskite $Sr_3Fe_2ReO_9$ phase has not been reported before. Based on a relaxed theoretical model that is consistent with the experimental images, density functional theory calculations are performed to determine the magnetic ground states and exchange parameters of the newly discovered $Sr_3Fe_2ReO_9$ phase, in which nearest-neighbour Fe and Re cations are coupled antiferromagnetically. This combination of aberration-corrected analytical TEM and *ab initio* calculations provides physical insight into cation order and magnetic coupling in perovskite oxides at the atomic level.

Key words: 1:2 B-site-ordered triple perovskite $Sr_3Fe_2ReO_9$, aberration-corrected transmission electron microscopy, antiferromagnetic coupling, cation order, density functional theory calculations

Introduction

Pseudo-cubic (pc) perovskite oxides with the formula $A(B_xB'_y)O_3$, where $x+y=1$ (e.g., $x=y=1/2$ or $x=2/3$, $y=1/3$) and A = Sr, Ba, Ca, or Mn; B = Fe, Co, Cr, Nb, Ir, or Sb; and B' = Re, Te, Mo, W, Mn, Ni, or Ca, have provided a playground for realizing tunable magnetic properties for several decades, as a wide spectrum of combinations of different cations is possible with different types of B-site cation ordering (Katz & Ward, 1964; Harari et al., 1974; James et al., 1995; Kobayashi et al., 1998; Viola et al., 2003; Augsburger et al., 2006; Zhao et al., 2009; King & Woodward, 2010; Hwang et al., 2012; Lee et al., 2014; Vasala & Karppinen, 2015; Tang et al., 2016; Bijelić et al., 2020; Solana-Madruga et al., 2021; Kojčinović et al., 2022). One of the most frequent types of cation ordering at B sites in $A(B_xB'_y)O_3$ is 1:1 rock-salt ordering, in which two cation layers located at crystallographically equivalent sixfold-coordinated sites B_1 and B_2 with 1:1 layering alternate along $[111]_{pc}$ with an ordering vector of 1/2[111]* in a NaCl-type arrangement (Nakamura & Choy, 1977). In the rock-salt-ordered double perovskite, the B_1 and B_2 sites can be occupied by individual B or B' species, or by a combination of B and B' species in certain ratios. The crystallographic formula of rock-salt-ordered double perovskite oxides $A(B_xB'_y)O_3$ can be written in the form $A[B_\mu/B'_\nu]_{B_1}[B_{x-\mu}/B'_{y-\nu}]_{B_2}O_3$, where $0\le\mu\le x$, $0\le\nu\le y$ and $x+y=1$. Besides the commonly known rock-salt-ordered double perovskite, there are other families of 1:2 B-site-ordered triple perovskites, in which cation layers are located at three crystallographically equivalent sixfold-coordinated sites B_1, B_2, and B_3, with 1:2 layering along $[111]_{pc}$ and an ordering vector of 1/3[111]* (Galasso et al., 1961; Woodward, 1997; Davies, 1999; Park & Woodward, 2000; Howard & Stokes, 2004; Ting et al., 2004*a*, 2004*b*; Rijssenbeek et al., 2005; Davies et al., 2008; Zhao et al., 2009; Hwang et al., 2012; Lee et al., 2014; Tang et al., 2016; Solana-Madruga et al., 2021). In the case of two magnetic B-site cations, all short-range B–O–B', long-range B–O–B'–O–B, and B'–O–B–O–B'

Received: March 14, 2022. **Revised:** September 7, 2022. **Accepted:** September 29, 2022

interactions are extremely sensitive to the type and degree of ordering, as well as to the occupancy of the B-site cations (Vasala & Karppinen, 2015). In $SrFe_xTe_yO_3$, rock-salt-ordered $Sr[Fe_{0.36}Te_{0.14}]_{B_1}[Fe_{0.305}Te_{0.195}]_{B_2}O_3$, *i.e.*, $Sr_3Fe_2TeO_9$, exhibits ferrimagnetic ordering below ~260 K with ~0.03 μ_B per Fe atom at 50 K (Ivanov et al., 2007), while rock-salt-ordered $Sr[Fe_{0.45}Te_{0.05}]_{B_1}[Fe_{0.285}Te_{0.215}]_{B_2}O_3$ exhibits ferrimagnetic ordering below ~717 K with ~0.8 μ_B per Fe atom at 2 K (Augsburger et al., 2006) and 0.0054 μ_B per Fe atom at 300 K (Kojčinović et al., 2022).

More interestingly, another phase of $Sr_3Fe_2TeO_9$ is found in the form of $Sr_3[Fe]_{B_1}[Fe]_{B_2}[Te]_{B_3}O_9$ with a 1:2 B-site-ordered triple perovskite structure. This yields a hexagonal superstructure, in which Fe and Te cations have a layer repeat of –[Fe–Fe-Te]$_n$– along $[111]_{pc}$, corresponding to antiferromagnetic (AFM) ordering at room temperature (Tang et al., 2016). In $SrFe_xRe_yO_3$, rock-salt-ordered $Sr_2[Fe]_{B_1}[Re]_{B_2}O_6$ exhibits ferrimagnetic ordering below ~419 K with an estimated 2.24 μ_B per formula unit at 0 K, while rock-salt-ordered $Sr_2[Fe]_{B_1}[Fe_{13}Re_{23}]_{B_2}O_6$, *i.e.*, $Sr_3Fe_2ReO_9$, exhibits ferrimagnetic ordering below ~475 K with a lower saturation moment (Abe et al., 1973; Ivanov et al., 2007). Another $Sr_3Fe_2ReO_9$ phase has been identified as rock-salt-ordered $Sr_2[Fe_{0.57}Re_{0.43}]_{B_1}[Fe_{0.76}Re_{0.24}]_{B_2}O_6$, exhibiting ferrimagnetic ordering below 450 K and a saturation magnetization of 1.10 μ_B/mol (Pannunzio Miner et al., 2007). The ordering type and occupancy of B-site cations therefore appear to significantly affect the magnetic properties of perovskite oxides, even if their nominal stoichiometry is similar or even the same. It should be noted that cation order and site occupancy in most of the perovskite oxides mentioned above were determined from Rietveld refinement of neutron powder diffraction or powder X-ray diffraction measurements, meaning that the crystallographic information was averaged spatially. However, the presence of nanoscale inhomogeneities in ordering, elemental segregation, secondary phases, and site occupancy in such perovskite oxides highlights the need for characterization techniques that can achieve atomic spatial resolution.

A transmission electron microscope (TEM) can provide atomic-scale information about atomic positions and elemental composition in materials. In particular, the advent of spherical aberration (C_S) correction has made it possible to measure the positions and occupancies of individual atomic columns (Haider et al., 1998; Jia et al., 2003). By combining aberration-corrected (AC) scanning TEM (STEM) with energy-dispersive X-ray spectroscopy (EDS), the type and degree of B-site cation ordering in double and triple perovskite oxides has been determined at the atomic scale (Lim et al., 2016; Wang et al., 2018). In our previous work, the cation ratio and ordering of two nanosized phases in polycrystalline $Sr_2Fe_{1+x}Re_{1-x}O_6$ with Re deficiency was determined experimentally to comprise a rock-salt-ordered double perovskite $Sr_2[Fe]_{B_1}[Fe_{0.2}Re_{0.8}]_{B_2}O_6$ and a disordered perovskite $Sr[Fe_{0.8}Re_{0.2}]O_3$ by using AC STEM and EDS (Ho et al., 2018).

Here, we identify a nanosized $Sr_3Fe_2ReO_9$ phase that has a 1:2 B-site-ordered triple perovskite structure and is buried in polycrystalline $Sr_2Fe_{1+x}Re_{1-x}O_6$ with Re deficiency by using AC STEM. In comparison to $Sr_2[Fe]_{B_1}[Re]_{B_2}O_6$ with a rock-salt-ordered double perovskite structure, which we use as a benchmark sample, the ordering type, elemental site occupancy and valence state of the B-site cations in a 1:2 B-site-ordered triple perovskite $Sr_3Fe_2ReO_9$ is investigated using high-angle annular dark-field (HAADF) STEM, EDS, electron energy-loss spectroscopy (EELS) and nanodiffraction. To the best of our knowledge, this 1:2 B-site-ordered triple perovskite phase of $Sr_3Fe_2ReO_9$ has not been reported before. Different possible magnetic structures of the 1:2 B-site-ordered triple perovskite $Sr_3Fe_2ReO_9$ phase are compared, in order to determine the magnetic ground states and exchange parameters, by performing first principles calculations. In order to confirm the validity of the theoretical model, HAADF STEM simulations are compared with the experimental images.

Materials and Methods

Polycrystalline samples of $Sr_2Fe_{1+x}Re_{1-x}O_6$ and Sr_2FeReO_6 were synthesized using a conventional solid-state method and spark plasma sintering (SPS; Sumitomo Coal Mining SPS-1050). The $Sr_2Fe_{1+x}Re_{1-x}O_6$ sample with Re deficiency was prepared with a nominal stoichiometric ratio of $SrCO_3$, Fe_2O_3 and ReO_3 powders, which were mixed by ball milling and pressed into pellets for the precursors. The Sr_2FeReO_6 sample without Re deficiency was prepared with 15 mol% Re excess, in order to compensate for the volatility of Re. TEM specimens were prepared using conventional methods, including mechanical grinding, dimpling and polishing. Finally, Ar ion milling was carried out on a Bal-Tec Res-101 system.

Atomic-resolution HAADF STEM imaging with a probe current of 80 pA and a semi-convergence angle of 22–24 mrad was performed at an accelerating voltage of 300 kV using an FEI Titan 80–300 microscope equipped with a three-condenser-lens system, a monochromator unit and a C_S probe corrector (CEOS). EDS elemental mapping was carried out at an accelerating voltage of 200 kV using an FEI 80–200 probe-AC ChemiSTEM microscope, which has a STEM spatial resolution of 80 pm and is equipped with a high brightness field emission gun and a Super-X EDS system comprising four Si drift detectors with an energy resolution of <136 eV @ Mn K_α (10 kcps). Datasets were recorded for 20–30 min with at least 1,024 × 768 pixels and processed using Bruker Esprit software. Statistical analysis of cation compositions was obtained from elemental maps recorded over regions of several tens of nm in size for arbitrary grain orientations.

Total energy calculations were performed using density functional theory (DFT), as implemented in the Vienna Ab initio Simulation Package (VASP) (Kresse & Furthmüller, 1996). Projector augmented wave (PAW) (Gajdoš et al., 2006) potentials were implemented in VASP. The Perdew Burke-Ernzerhof (PBE) (Perdew et al., 1996) exchange-correlation functional of the generalized gradient approximation (GGA) was selected. A 7 × 7 × 2 k-point mesh in the first irreducible Brillouin zone (BZ) was generated *via* the Monkhorst–Pack method after convergence tests. The convergence criteria were set as follows: 10^{-6} eV for total energy and 0.01 GPa for maximum stress. The cut-off energy was set to 550 eV, in order to ensure the accuracy of the calculation, while a quasi-Newton algorithm was applied for initial geometric optimization. Spin polarization was considered. The GGA plus on-site repulsion U (GGA + U) method was employed with $U = 4$ eV, $J = 0.89$ eV on Fe and $U = 2$ eV, $J = 1$ eV on Re. Here, U denotes on-site Coulomb repulsion, while

J denotes the exchange interaction in the Hubbard model. Based on DFT-relaxed theoretical models, HAADF STEM image simulations were performed using the multi-slice method implemented in the MULTEM image simulation software package (Lobato & Van Dyck, 2015).

Results and Discussion

Figure 1a shows a HAADF STEM image of a 1:2 B-site-ordered triple perovskite $Sr_3Fe_2ReO_9$ phase with a size of ~30 nm in the polycrystalline $Sr_2Fe_{1+x}Re_{1-x}O_6$ sample with Re deficiency. A nanodiffraction pattern, as shown in Figure 1b, was recorded along $\langle 011\rangle_{pc}$ from the sample area indicated by a red disk in Figure 1a. The nanodiffraction pattern shows fractional super-reflection spots such as $\frac{1}{3}\{\bar{1}1\bar{1}\}_{pc}$ and $\frac{2}{3}\{\bar{1}1\bar{1}\}_{pc}$, as indicated by yellow triangles, demonstrating the formation of a triple periodicity along $\langle\bar{1}1\bar{1}\rangle_{pc}$ in $Sr_3Fe_2ReO_9$. In comparison, Figures 1c and 1d show a HAADF STEM image and a nanodiffraction pattern, respectively, recorded from a double perovskite Sr_2FeReO_6 grain in the polycrystalline Sr_2FeReO_6 sample without Re deficiency. The nanodiffraction pattern recorded from the rock-salt-ordered double perovskite Sr_2FeReO_6 shows half-integer super-reflection spots such as $\frac{1}{2}\{\bar{1}1\bar{1}\}_{pc}$, as indicated by green triangles, demonstrating the formation of a double periodicity along $\langle\bar{1}1\bar{1}\rangle_{pc}$ in Sr_2FeReO_6. The presence of half-integer super-reflection spots in the nanodiffraction pattern recorded from the $Sr_3Fe_2ReO_9$ region shown in Figure 1b may be attributed to slight overlap between the 1:2 B-site-ordered triple perovskite and 1:1 B-site-ordered double perovskite phases in the incident electron beam direction. The fraction of the 1:2 B-site-ordered triple perovskite $Sr_3Fe_2ReO_9$ phase in the polycrystalline $Sr_2Fe_{1+x}Re_{1-x}O_6$ sample is extremely low in the field of view, as shown in a low-magnification HAADF STEM image in Supplementary Figure S1, resulting in the absence of a characteristic diffraction peak from a 1:2 B-site-ordered triple perovskite $Sr_3Fe_2ReO_9$ phase in XRD patterns recorded from a bulk sample (*c.f.* Supplementary Figure S2).

The atomic-resolution HAADF STEM images of the $Sr_3Fe_2ReO_9$ and Sr_2FeReO_6 phases viewed along $\langle 011\rangle_{pc}$ shown in Figures 2a and 2c, respectively, reveal atomic columns of SrO in green, Fe in red and Re in blue, based on Z contrast intensity differences between each column. The intensities of the Fe columns are weakest, while the intensities of the Re columns are strongest. The presence of –[Fe–Fe–Re]$_n$– ordering at B_1, B_2 and B_3 sites in the 1:2 B-site-ordered triple perovskite lattice in the horizontal direction, as indicated by blue triangles, is revealed in Figure 2a. In comparison, –[Fe–Re]$_n$– ordering is present at B_1 and B_2 sites in the double perovskite lattice in the horizontal direction, as indicated by red triangles in Figure 2c.

As no crystallographic information about the newly discovered 1:2 B-site-ordered $Sr_3Fe_2ReO_9$ phase is currently

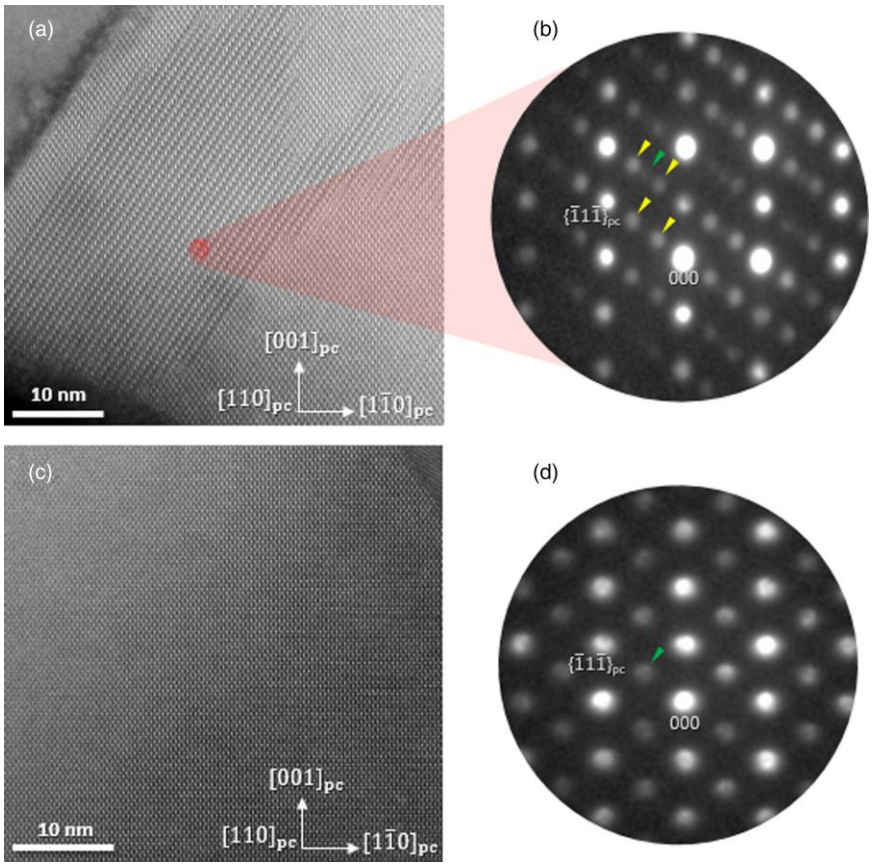

Fig. 1. High-angle annular dark-field scanning transmission electron microscopy images and nanodiffraction patterns of (**a**, **b**) the 1:2 B-site-ordered triple perovskite $Sr_3Fe_2ReO_9$ and (**c**, **d**) the 1:1 B-site-ordered double perovskite Sr_2FeReO_6 viewed along $\langle 011\rangle_{pc}$ in pseudo-cubic (pc) notation. Fractional super-reflection spots (such as $\frac{1}{3}\{\bar{1}1\bar{1}\}_{pc}$) and half-integer super-reflection spots (such as $\frac{1}{2}\{\bar{1}1\bar{1}\}_{pc}$) are indicated by yellow and green triangles, respectively.

available in the crystallographic database and publications, we built models for the 1:2 B-site-ordered $Sr_3Fe_2ReO_9$ triple perovskite based on the two possible crystallographic structures of 1:2 B-site-ordered $Sr_3Fe_2ReO_9$ triple perovskite and the similarity in radii and valence states of the Re^{6+} and Te^{6+} cations. The model with space group $P\bar{3}m1$ corresponds to $Sr_3Fe_2TeO_9$ from the 'Materials Projects' dataset (Jain et al., 2013), while the model with space group $P\bar{3}c1$ corresponds to $Sr_3Fe_2TeO_9$ from the publication of Tang et al. (2016). Figures 2b and 2d show three-dimensional (3D) models of the crystal structures of double perovskite Sr_2FeReO_6 and triple perovskite $Sr_3Fe_2ReO_9$ with space group $P\bar{3}m1$, respectively. Simulated electronic diffraction patterns of $Sr_3Fe_2ReO_9$ with space group $P\bar{3}m1$ and $P\bar{3}c1$ along various low-index zone axes, as shown in Figure S3, demonstrate that along $[1\bar{1}0]$, rather than [100], [001], [110] or [111], the two space groups $P\bar{3}m1$ and $P\bar{3}c1$ can be distinguished from each other by comparing the additional super-reflection spots indicated by yellow arrows. Our experimental electron diffraction patterns and STEM images recorded along $\langle 011\rangle_{pc}$ (which corresponds to [100] here) in Figures 1 and 2 cannot be used to distinguish the two space groups. Unfortunately, this nanosized $Sr_3Fe_2ReO_9$ phase, as an impurity in $Sr_2Fe_{1+x}Re_{1-x}O_6$, cannot be tilted to $[1\bar{1}0]$ due to the limited tilt range of the sample holder and the relatively large angles between [100] and the other characteristic crystallographic directions. The 1:2 B-site-ordered $Sr_3Fe_2ReO_9$ phases with space groups $P\bar{3}m1$ and $P\bar{3}c1$ are both considered in the DFT calculation described below. Based on DFT-relaxed theoretical models of the 1:2 B-site-ordered triple perovskite $Sr_3Fe_2ReO_9$ with space groups $P\bar{3}m1$ and $P\bar{3}c1$, we performed HAADF STEM image simulations under the experimental acquisition conditions. Simulated images based on $Sr_3Fe_2ReO_9$ with space groups $P\bar{3}m1$ and $P\bar{3}c1$ are shown in the green dotted boxes at the top left corners of Figure 2a and Figure S4 and are consistent with the experimental image, confirming the validity of the theoretical model of the 1:2 B-site-ordered triple perovskite $Sr_3Fe_2ReO_9$ predicted by DFT calculations. Similarly, a simulated image of the double perovskite Sr_2FeReO_6 shown in Figure 2c is consistent with the corresponding experimental image. Atomic models of 1:2 B-site-ordered $Sr_3Fe_2ReO_9$ with space group $P\bar{3}m1$ superimposed on Figures 2a and 2c show Sr in green, Fe in red and Re in blue.

Fe/Re cation order on the atomic scale was investigated by using EDS elemental mapping of the Fe K_α signal at 6.405 keV and the Re K_α signal at 8.652 keV, with a spectrum region from 0 to 10 keV (*c.f.* Supplementary Figure S5). The atomic-resolution compositional color maps shown in Figure 3 reveal that Fe atoms in red (*c.f.* Figures 3a and 3e) and Re atoms in blue (*c.f.* Figures 3b and 3f) on B sites in $Sr_3Fe_2ReO_9$ and Sr_2FeReO_6 stack alternately in –[Fe–Fe–Re]$_n$– (*c.f.* Figure 3d) and –[Fe–Re]$_n$– (*c.f.* Figure 3 h) order, respectively. These features are consistent with the Z contrast images shown in Figure 2. No significant anti-site occupation between Fe atoms on the B_1 and B_2 sites and Re atoms on the B_3 sites is observed in $Sr_3[Fe]_{B_1}[Fe]_{B_2}[Re]_{B_3}O_9$. Our statistical EDS measurements of the cation ratio of Fe to Re on the B sites indicate an Fe/Re ratio of 0.67:0.33 in $Sr_3Fe_2ReO_9$ with a standard deviation of $\sigma < 0.01$ and an Fe/Re ratio of 0.52:0.48 in Sr_2FeReO_6 with $\sigma \leq 0.01$. Furthermore, Supplementary

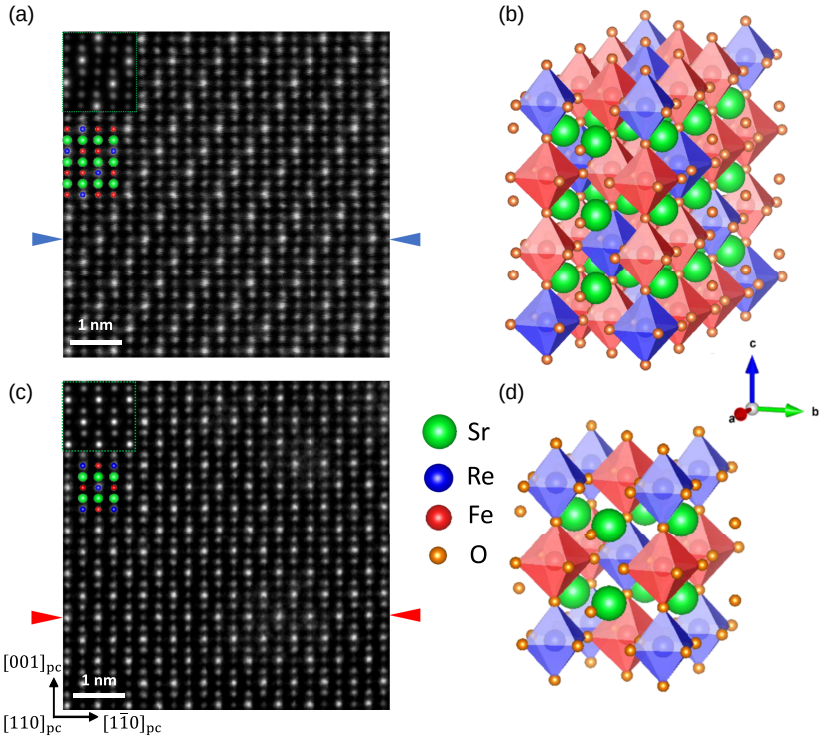

Fig. 2. Atomic-resolution high-angle annular dark-field scanning transmission electron microscopy (HAADF STEM) images viewed along $\langle 011\rangle_{pc}$ and schematic crystal structures of (**a**, **b**) the 1:2 B-site-ordered triple perovskite $Sr_3Fe_2ReO_9$ with space group $P\bar{3}m1$ and (**c**, **d**) the 1:1 B-site-ordered double perovskite Sr_2FeReO_6. Atomic models with Fe in red, Sr in green, Re in blue and O in orange, as well as simulated HAADF STEM images, are superimposed on the experimental images as insets.

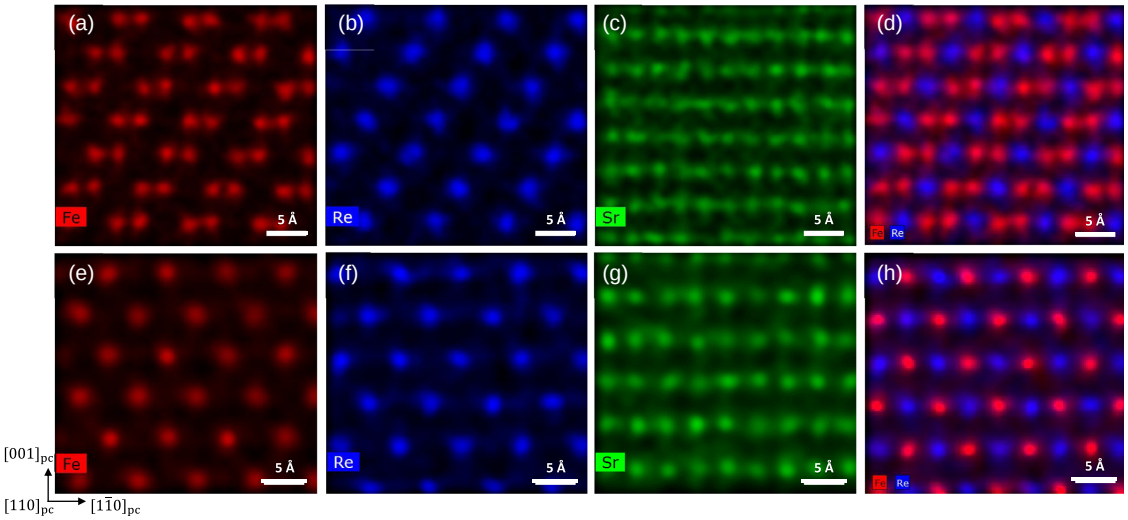

Fig. 3. Atomic-resolution elemental mapping of (**a–d**) the 1:2 B-site-ordered triple perovskite $Sr_3Fe_2ReO_9$ and (**e–h**) the double perovskite Sr_2FeReO_6 viewed along $\langle 011 \rangle_{pc}$, with (**a**, **e**) Fe in red, (**b**, **f**) Re in blue, (**c**, **g**) Sr in green, and (**d**, **h**) mixed Fe and Re maps in red and blue.

Figure S6 shows almost identical experimental electron energy-loss near-edge fine structures for the Fe $L_{3,2}$ edges in $Sr_3Fe_2ReO_9$ and Sr_2FeReO_6, confirming the presence of similar trivalent states of the Fe^{3+} cations in the $Sr_2^{2+}[Fe^{3+}]_{B_1}[Re^{5+}]_{B_2}O_6^{2-}$ and $Sr_3^{2+}[Fe^{3+}]_{B_1}[Fe^{3+}]_{B_2}[Re^{6+}]_{B_3}O_9^{2-}$ phases.

In order to understand the magnetic coupling between the ordered B-site cations in the 1:2 B-site-ordered triple perovskite $Sr_3Fe_2ReO_9$, DFT calculations were performed to evaluate the formation energy E_{form} of the 1:2 B-site-ordered triple perovskite $Sr_3Fe_2ReO_9$ for the various magnetic structures presented in Table 1. The two types of 1:2 B-site-ordered $Sr_3Fe_2ReO_9$ triple perovskite described above, with either $P\bar{3}m1$ or $P\bar{3}c1$ symmetry, as well as a ferromagnetic (FM) structure and five AFM structures denoted AFM1-AFM5, as illustrated in Supplementary Figure S7, were considered in the DFT calculations. E_{form} was computed from the following equation:

$$E_{form} = \frac{[E(compound) - E(atoms)]}{n} \quad (1)$$

where E(compound) and E(atoms) denote the ground state energies of the perovskite and isolated atoms, respectively, considering spin polarisation. A lower formation energy indicates better structural stability. As listed in Table 1, the paramagnetic (PM) states have higher E_{form} and are less stable than the AFM and FM states. In each 1:2 B-site-ordered $Sr_3Fe_2ReO_9$ triple perovskite with space group $P\bar{3}m1$ and $P\bar{3}c1$, the most stable ground state is the AFM2 state, in which all of the nearest-neighbour Fe and Re cations are coupled antiferromagnetically, as shown in Figure 4. Fe atoms between adjacent $[111]_{pc}$ planes exhibit AFM coupling, in agreement with the magnetic structure of the 1:2 B-site-ordered $Sr_3Fe_2TeO_9$ triple perovskite obtained by Tang et al. (2016). $Sr_3Fe_2ReO_9$ with space group $P\bar{3}m1$ and the AFM2 state has the lowest formation energy, whereas $Sr_3Fe_2ReO_9$ with space group $P\bar{3}c1$ and the AFM2 state has a formation energy that is 8.2 meV/atom higher than that for $P\bar{3}m1$ symmetry. Here, the $P\bar{3}m1$ phase was used to perform further DFT calculations of the exchange parameter J_{ij}. After geometrical optimization, the lengths of the a, b and c axes in the DFT-relaxed $Sr_3Fe_2ReO_9$ model with space group $P\bar{3}m1$ are 5.613, 5.613 and 6.913 Å, respectively.

After taking spin-orbit coupling (SOC) interactions into consideration, J_{ij} was calculated for the ground state of the 1:2 B-site-ordered $Sr_3Fe_2ReO_9$ triple perovskite using the 'four-state method'. More details about the 'four-state method' are available elsewhere (Xiang et al., 2013; Li et al., 2021). The six kinds of interactions between pairs of nearest-neighbour magnetic cations connected by oxygen anions in the 1:2 B-site-ordered triple perovskite $Sr_3Fe_2ReO_9$ are indicated as 1–6 in Figure 4. The Heisenberg spin Hamiltonian was adopted according to the following equation:

$$H_{spin} = \sum_{ij} J_{ij} S_i S_j, \quad (2)$$

where J_{ij} and S denote the exchange coupling parameter and spin vector, respectively. A positive value of the exchange parameter J_{ij} represents AFM coupling and *vice versa*. As listed in Figure 4, all of the calculated J_{ij} parameters are positive, demonstrating that all of the nearest-neighbor cations are coupled antiferromagnetically. This finding is consistent with the predicted AFM2 ground state.

Table 1. Formation energy of 1:2 B-site-ordered $Sr_3Fe_2ReO_9$ triple perovskite with $P\bar{3}c1$ and $P\bar{3}m1$ space groups (eV/atom).

Space group	PM	FM	AFM1	AFM2	AFM3	AFM4	AFM5
$P\bar{3}c1$	−5.2468	−5.5027	−5.2548	−5.5156	−5.4106	−5.2998	−5.2681
$P\bar{3}m1$	−5.2409	−5.4963	−5.5187	−5.5234	−5.5193	−5.4967	−5.4968

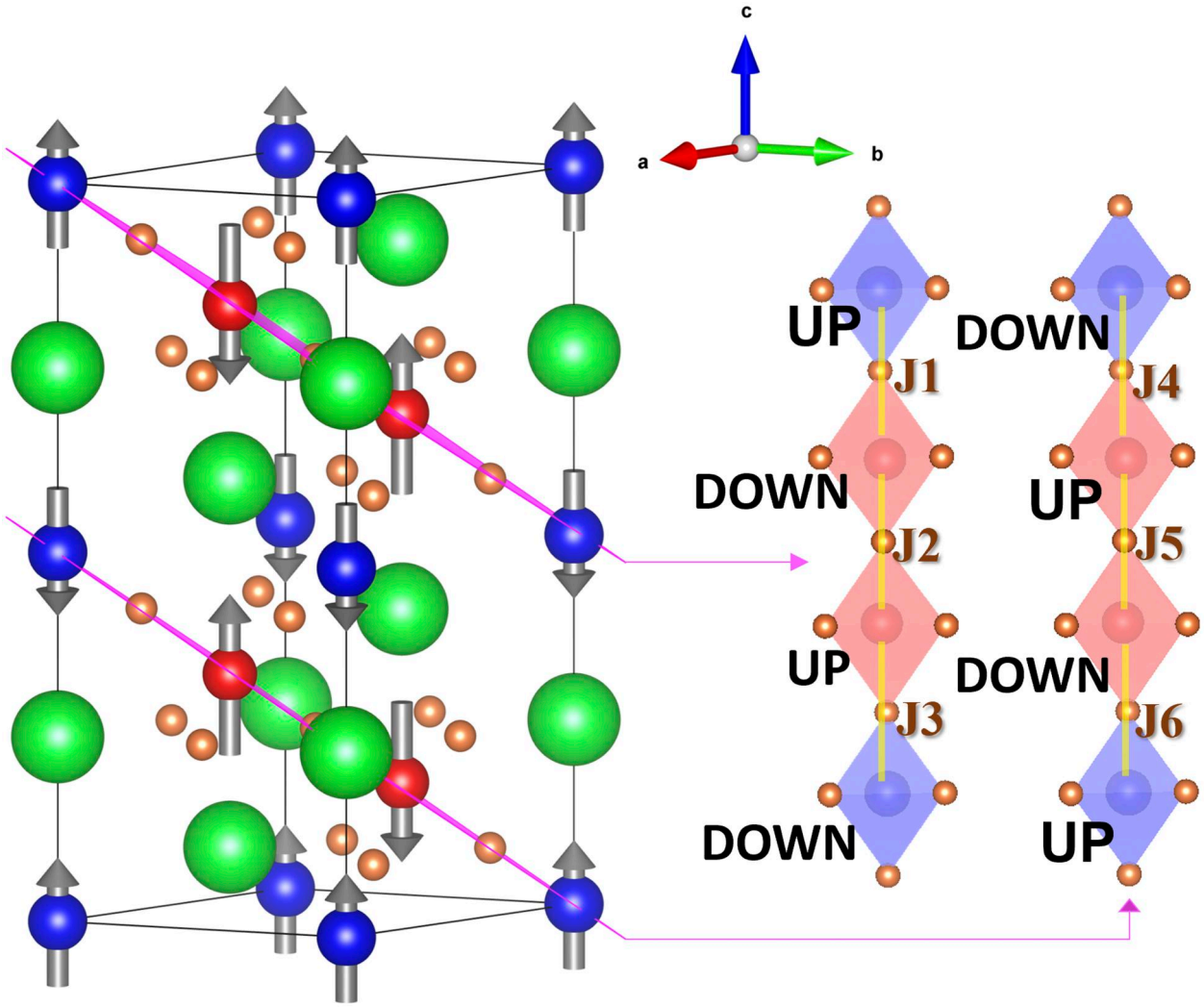

Fig. 4. Magnetic ground states and exchange parameters (J_{ij}) of the 1:2 B-site-ordered triple perovskite $Sr_3Fe_2ReO_9$, with O atoms in orange, Fe atoms in red, Sr atoms in green and Re atoms in blue. The directions and lengths of the grey arrows indicate the directions and magnitudes, respectively, of the magnetic moments. 1 to 6 represent six kinds of interactions between pairs of nearest-neighbour magnetic cations connected by oxygen anions in the 1:2 B-site-ordered triple perovskite $Sr_3Fe_2ReO_9$.

Conclusions

A $Sr_3Fe_2ReO_9$ phase with a 1:2 B-site-ordered triple perovskite structure has been discovered and investigated using AC TEM. The atomic arrangement, cation order, valence states and elemental site occupancy have been obtained experimentally on the atomic scale from an individual nano-sized region of the $Sr_3Fe_2ReO_9$ phase. At three crystallographically equivalent B_1, B_2 and B_3 sites in $Sr_3[Fe]_{B_1}[Fe]_{B_2}[Re]_{B_3}O_9$, Fe and Re cations stack alternately in $-[Fe–Fe–Re]_n-$ order without any significant anti-site occupation. The magnetic ground states and exchange parameters of this newly discovered $Sr_3Fe_2ReO_9$ phase, as determined by DFT calculations, reveal that all of the nearest-neighbour Fe and Re cations are coupled *via* AFM Fe–O–Fe or Fe–O–Re exchange interactions. The combination of AC TEM and DFT calculations that we use provides an atomic-level understanding of the relationship between cation order and magnetic coupling in complex perovskite oxides.

Supplementary material

To view supplementary material for this article, please visit https://doi.org/10.1093/micmic/ozac011.

Acknowledgments

This paper is dedicated to celebrating the 25th anniversary of the function and publication of the world's first aberration-corrected transmission electron microscope, which revolutionized the study of electron microscopy and spectroscopy, at the PICO 2022 Conference.

Financial support

This work was financially supported by National Natural Science Foundation of China (52171014, 52011530124), Science, Technology and Innovation Commission of Shenzhen Municipality (HZQB-KCZYB-2020031, SGDX20210823104200001, JCYJ20210324134402007),

the Sino-German Mobility Program by the Sino-German Center for Research Promotion (M-0265), Science and Technology Department of Sichuan Province (2021YFSY0016), Innovation and Technology Fund (ITS/365/21), CityU Strategic Interdisciplinary Research Grant (7020016, 7020043), the City University of Hong Kong (Project nos 9610484, 9680291, 9678288, 9360162, 9610558) and the City University of Hong Kong Shenzhen Research Institute. The work described in this paper was substantially supported by a grant from the EU-HK Research and Innovation Cooperation Co-funding Mechanism sponsored by the Research Grants Council of Hong Kong Special Administrative Region, China (Project No. E-CityU101/20), Germany/Hong Kong Joint Research Scheme (DAAD-RGC) (Project No. G-CityU102/20) and the Research Grants Council of the Hong Kong Special Administrative Region, China (Project No. CityU 11302121, 11309822). This project has received funding from the European Research Council (ERC) under the European Union's Horizon 2020 research and innovation program (Grant No. 856538, project "3D MAGiC") and from the Deutsche Forschungsgemeinschaft (project number 392476493). P.-L.H is grateful for funding from the Swire Charitable Trust (University College Oxford), Raymond Liang (Primax Electronics Ltd) and Ministry of Education (Taiwan). This work made use of the resources of the Ernst Ruska-Centre for Microscopy and Spectroscopy with Electrons in Forschungszentrum Jülich, the National Centre for Electron Microscopy in Beijing and the TRACE EM center at the City University of Hong Kong. The authors thank Jing Zhu, Peter D. Nellist, Fu-Rong Chen, Jiayi Li, Mathias Rothmann, Zheying Xu, Kyung Song and James P. Buban for valuable contributions to this work.

Conflict of interest

The authors declare that they have no competing interest.

References

Abe M, Nakagawa T & Nomura S (1973). Magnetic and Mössbauer studies of the ordered perovskites Sr2Fe1 + xRe1-xO6. *J Phys Soc Japan* **35**(5), 1360–1365.

Augsburger MS, Viola MC, Pedregosa JC, Carbonio RE & Alonso JA (2006). Crystal structure and magnetism of the double perovskites Sr3Fe2TeO9 and Ba3Fe2TeO9: a neutron diffraction study. *J Mater Chem* **16**(43), 4235–4242.

Bijelić J, Stanković A, Medvidović-Kosanović M, Marković B, Cop P, Sun Y, Hajra S, Sahu M, Vukmirović J, Marković D, Kukovecz Á, Jagličić Z, Smarsly BM & Djerdj I (2020). Rational sol–gel-based synthesis design and magnetic, dielectric, and optical properties study of nanocrystalline Sr3Co2WO9 triple perovskite. *J Phys Chem C* **124**(23), 12794–12807.

Davies PK (1999). Cation ordering in complex oxides. *Curr Opin Solid State Mater Sci* **4**(5), 467–471.

Davies PK, Wu H, Borisevich AY, Molodetsky IE & Farber L (2008). Crystal chemistry of complex perovskites: new cation-ordered dielectric oxides. *Annu Rev Mater Res* **38**(1), 369–401.

Gajdoš M, Hummer K, Kresse G, Furthmüller J & Bechstedt F (2006). Linear optical properties in the projector-augmented wave methodology. *Phys Rev B* **73**(4), 045112.

Galasso F, Barrante JR & Katz L (1961). Alkaline earth-tantalum-oxygen phases including the crystal structure of an ordered perovskite compound, Ba3SrTa2O9. *J Am Chem Soc* **83**(13), 2830–2832.

Haider M, Uhlemann S, Schwan E, Rose H, Kabius B & Urban K (1998). Electron microscopy image enhanced. *Nature* **392**(6678), 768–769.

Harari D, Poix P & Bernier JC (1974). Etude structurale de quatre nouvelles pérovskites au cobalt. *J. Solid State Chem* **11**(4), 330.

Ho P-L, Yu C-P, Zhang Q, Song K, Buban JP, Choi S-Y, Dunin-Borkowski RE, Mayer J, Tai N-H, Zhu J, Jin L & Zhong X (2018). Effect of cation ratio and order on magnetic circular dichroism in the double perovskite Sr2Fe1 + xRe1-xO6. *Ultramicroscopy* **193**, 137–142.

Howard CJ & Stokes HT (2004). Octahedral tilting in cation-ordered perovskites - a group-theoretical analysis. *Acta Crystallographica Section B* **60**(6), 674–684.

Hwang J, Choi ES, Ye F, Dela Cruz CR, Xin Y, Zhou HD & Schlottmann P (2012). Successive magnetic phase transitions and multiferroicity in the spin-one triangular-lattice antiferromagnet Ba3NiNb2O9. *Phys Rev Lett* **109**(25), 257205.

Ivanov SA, Nordblad P, Eriksson SG, Tellgren R & Rundlöf H (2007). The magnetoelectric perovskite Sr3Fe2TeO9: An insight from magnetic measurements and neutron powder diffraction. *Mater Res Bull* **42**(4), 776–789.

Jain A, Ong SP, Hautier G, Chen W, Richards WD, Dacek S, Cholia S, Gunter D, Skinner D, Ceder G & Persson KA (2013). Commentary: the materials project: a materials genome approach to accelerating materials innovation. *APL Mater* **1**(1), 011002.

James M, Attfield JP & Rodriguez-Carvajal J (1995). Synthesis, crystal structure and magnetism of Sr3Sb2NiO9—A ferrimagnetic perovskite. *J Phys Chem Solids* **56**(10), 1331–1337.

Jia CL, Lentzen M & Urban K (2003). Atomic-resolution imaging of oxygen in perovskite ceramics. *Science* **299**(5608), 870–873.

Katz L & Ward R (1964). Structure relations in mixed metal oxides. *Inorg Chem* **3**(2), 205–211.

King G & Woodward PM (2010). Cation ordering in perovskites. *J Mater Chem* **20**(28), 5785–5796.

Kobayashi KI, Kimura T, Sawada H, Terakura K & Tokura Y (1998). Room-temperature magnetoresistance in an oxide material with an ordered double-perovskite structure. *Nature* **395**(6703), 677–680.

Kojčinović J, Sahu M, Hajra S, Tatar D, Klaser T, Skoko Ž, Jagličić Z, Sadrollahi E, Litterst FJ, Kim HJ & Djerdj I (2022). Nanocrystalline triple perovskite compounds A3Fe2BO9 (A = Sr, Ba; B = W, Te) with ferromagnetic and dielectric properties for triboelectric energy harvesting. *Mater Chem Front* **6**, 1116–1128.

Kresse G & Furthmüller J (1996). Efficient iterative schemes for ab initio total-energy calculations using a plane-wave basis set. *Physical Review B* **54**(16), 11169–11186.

Lee M, Choi ES, Huang X, Ma J, Dela Cruz CR, Matsuda M, Tian W, Dun ZL, Dong S & Zhou HD (2014). Magnetic phase diagram and multiferroicity of Ba3MnNb2O9: A spin -5/2 triangular lattice antiferromagnet with weak easy-axis anisotropy. *Physical Review B* **90**-(22), 224402.

Li Z, Lu J, Jin L, Rusz J, Kocevski V, Yanagihara H, Kita E, Mayer J, Dunin-Borkowski RE, Xiang H & Zhong X (2021). Atomic structure and electron magnetic circular dichroism of individual rock salt structure antiphase boundaries in spinel ferrites. *Adv Funct Mater* **31**(21), 2008306.

Lim T-W, Kim S-D, Sung K-D, Rhyim Y-M, Jeen H, Yun J, Kim K-H, Song K-M, Lee S, Chung S-Y, Choi M & Choi S-Y (2016). Insights into cationic ordering in Re-based double perovskite oxides. *Sci Rep* **6**(1), 19746.

Lobato I & Van Dyck D (2015). MULTEM: a new multislice program to perform accurate and fast electron diffraction and imaging simulations using Graphics Processing Units with CUDA. *Ultramicroscopy* **156**, 9–17.

Nakamura T & Choy J-H (1977). Determination of ionic valency pairs via lattice constants in ordered perovskites (ALa)(Mn2 + Mo5+)O6 (A = Ba, Sr, Ca) with applications to (ALa)(Fe3 + Mo4+)O6, Ba2(Bi3 + Bi5+)O6 and Ba2(Bi3 + Sb5+)O6. *J Solid State Chem* **20**(3), 233–244.

Pannunzio Miner EV, De Paoli JM, Alonso JA, García-Hernández M, Sánchez RD & Carbonio RE (2007). Ferrimagnetic order in the insulating Sr3Fe2ReO9 double perovskite. *Physica B Condens Matter* **398**(2), 397–400.

Park J-H & Woodward PM (2000). Synthesis, structure and optical properties of two new Perovskites: Ba2Bi2/3TeO6 and Ba3Bi2TeO9. *Int J Inorg Mater* **2**(1), 153–166.

Perdew JP, Burke K & Ernzerhof M (1996). Generalized Gradient Approximation Made Simple. *Phys Rev Lett* **77**, 3865.

Rijssenbeek JT, Saito T, Malo S, Azuma M, Takano M & Poeppelmeier KR (2005). Effect of Explicit cationic size and valence constraints on the phase stability of 1:2 B-site-ordered perovskite ruthenates. *J Am Chem Soc* **127**(2), 675–681.

Solana-Madruga E, Ritter C, Aguilar-Maldonado C, Mentré O, Attfield JP & Arévalo-López ÁM (2021). Mn3MnNb2O9: high-pressure triple perovskite with 1 : 2 B-site order and modulated spins. *Chem Comm* **57**(68), 8441–8444.

Tang Y, Hunter EC, Battle PD, Sena RP, Hadermann J, Avdeev M & Cadogan JM (2016). Structural chemistry and magnetic properties of the perovskite Sr3Fe2TeO9. *J Solid State Chem* **242**, 86–95.

Ting V, Liu Y, Norén L, Withers RL, Goossens DJ, James M & Ferraris C (2004*a*). A structure, conductivity and dielectric properties investigation of A3CoNb2O9 (A = Ca2+, Sr2+, Ba2+) triple perovskites. *J Solid State Chem* **177**(12), 4428–4442.

Ting V, Liu Y, Withers RL & Norén L (2004*b*). An electron diffraction and bond valence sum study of the space group symmetries and structures of the photocatalytic 1:2 B site ordered A3CoNb2O9 perovskites (A = Ca2+, Sr2+, Ba2+). *J Solid State Chem* **177**(7), 2295–2304.

Vasala S & Karppinen M (2015). A2B′B″O6 perovskites: A review. *Prog Solid State Chem* **43**(1-2), 1–36.

Viola MDC, Augsburger MS, Pinacca RM, Pedregosa JC, Carbonio RE & Mercader RC (2003). Order–disorder at Fe sites in SrFe2/3B″1/3O3 (B″=Mo, W, Te, U) tetragonal double perovskites. *Solid State Chem* **175**(2), 252–257.

Wang Z, Tavabi AH, Jin L, Rusz J, Tyutyunnikov D, Jiang H, Moritomo Y, Mayer J, Dunin-Borkowski RE, Yu R, Zhu J & Zhong X (2018). Atomic scale imaging of magnetic circular dichroism by achromatic electron microscopy. *Nat Mater* **17**(3), 221–225.

Woodward PM (1997). Octahedral tilting in perovskites. I. Geometrical Considerations. *Acta Crystallogr B* **53**(1), 32–43.

Xiang H, Lee C, Koo H-J, Gong X & Whangbo M-H (2013). Magnetic properties and energy-mapping analysis. *Dalton Trans* **42**(4), 823–853.

Zhao JG, Yang LX, Yu Y, Li FY, Yu RC & Jin CQ (2009). Structural and physical properties of 1:2 B-site-ordered perovskite Ba3CaIr2O9. *J Solid State Chem* **182**(2), 327–330.